Photospheric and Coronal Currents in Solar Active Regions

Andrew B. Burnette and Richard C. Canfield

Department of Physics, Montana State University, Bozeman, MT 59717-3840, U.S.A.

canfield@physics.montana.edu

and

Alexei A. Pevtsov

National Solar Observatory/Sacramento Peak[1], PO Box 62, Sunspot, NM 88349, U.S.A.

apevtsov@nso.edu

ABSTRACT

Using photospheric line of sight magnetograms from the National Solar Observatory/Kitt Peak and coronal X-ray images from the Yohkoh Soft X-ray Telescope, we have determined the value of the constant α of the linear force-free-field model ($\nabla \times \mathbf{B} = \alpha \mathbf{B}$) that gives the best visual fit to the overall coronal X-ray structure (α_c) of 34 flare-productive active regions of relatively simple bipolar morphology. For 24 of these active regions vector magnetograms are available from the Haleakala Stokes Polarimeter at Mees Solar Observatory. For each of them we determine the single best-fit value of α in the photosphere (α_p) by three quite different methods, and show that these methods give statistically consistent values. By combining this dataset with that of NSO and SXT, we are able to compare for the first time quantitatively and statistically the observed values of α in the photosphere and corona of these regions. We find that the distribution of α_p and α_c values is fully consistent with the hypothesis that the overall twist density of the magnetic fields of active regions, as measured by the linear force-free field parameter α, is the same in the photosphere and the corona. We therefore conclude that the electric currents that create the non-potential structure of such solar coronal active regions are of sub-photospheric origin and pass without significant modification through the photosphere.

Subject headings: Sun: magnetic fields — Sun: corona — Sun: X-rays, gamma rays

---

[1]National Solar Observatory (NSO) is operated by the Association of Universities for Research in Astronomy (AURA, Inc) under cooperative agreement with the National Science Foundation (NSF).

1. INTRODUCTION

The topology of coronal magnetic fields plays important role in understanding solar flare phenomena and coronal heating. Still, direct measurements of coronal fields are very limited. In recent years sophisticated research has been carried out in which coronal magnetic field models have been derived through nonlinear force-free-field extrapolation of photospheric vector magnetograms, and subsequently compared with observations (Lee *et al.* 1998; Lee *et al.* 1999; Regnier *et al.* 2002). More commonly, however, photospheric magnetograms are extrapolated into corona using the much simpler linear force-free model, in which α is constant. A value of α suitable for this purpose can be determined by minimizing the difference between observed and computed horizontal photospheric fields (Pevtsov *et al.* 1995). When no vector magnetograms are available, fitting field lines extrapolated from line-of-sight magnetograms to coronal structures is often used to determine the value of α (Aurass *et al.* 1999; López Fuentes *et al.* 2000; Pevtsov *et al.* 2003).

In an earlier paper (Pevtsov *et al.* 1997) we represented obvious sigmoids in images from the Yohkoh Soft X-Ray Telescope (SXT, Tsuneta *et al.* 1991) using a simple two-dimensional linear force-free-field model. We showed that there is a correlation between these 2D values of α in the corona and the best-fit values of α in the photosphere. This result motivated Longcope and Welsch (2000) to investigate the relationship between these quantities theoretically. Modeling the emergence of a current-carrying flux tube into the corona, they found that about a day was required for the coronal value of α to equilibrate. Observations of active regions undergoing flux emergence that start from the very beginning of the emergence process have shown temporal dependence on such a time scale (Pevtsov *et al.* 2003), but observations more than a day or so after this time have revealed no significant variation (Wang and Abramenko 2000), despite continued flux emergence. The work reported below does not bear on this matter, since only two of the 47 observations in our dataset were made within two days of the beginning of emergence. On the other hand, Longcope and Welsch (2000) showed that that once equilibration is complete, the values of α in the corona saturate to those in the photosphere. This is therefore the hypothesis that we test in this work: *the twist of the magnetic fields of active regions in the corona has the same value as that in the photosphere.* We test this hypothesis using a fully 3D approach which allows us, for the first time, to make a quantitative comparison of photospheric and coronal α values for a dataset that is large enough to produce meaningful statistics.

A side issue in this paper is that of the uniformity of α in the corona. Vector magnetograms are often used to compute the point-to-point (x,y) variation in the photosphere of $\alpha_z \equiv \alpha(x,y) \equiv \mu J_z(x,y)/B_z$ (x,y)), where B_z is the vertical magnetic field, J_z is the vertical current density (both in the heliographic coordinate system), and $\mu = 4\pi \times 10^{-3}\, G\, m\, A^{-1}$

(Krall *et al.* 1982; Hagyard 1987; Pevtsov *et al.* 1994). These computations typically show large local fluctuations of α_z within active regions, including patches of both signs. The presence of these patches, as well as other factors, rules out a linear force-free model close to the photosphere. It is not surprising that there is only limited observational evidence for similar patterns in the corona (Levine 1976). In the presence of magnetic reconnection, we would expect the coronal field to simplify while conserving magnetic helicity (Taylor 1974; Taylor 1986; Berger 1999). Observational evidence that such relaxation may be taking place has recently been provided by Nandy *et al.* (2003).

The other side issue explored in this paper is the determination of the best methodology for establishing a single value of α, for an active region as a whole, from vector magnetograph data. Leka and Skumanich (1999) and Leka (1999) have compared three methods, and applied them to a single active region: α_{best}, the single value of α, based on the observed longitudinal magnetogram, that best fits the horizontal field of the corresponding vector magnetogram in a least squares sense (Pevtsov *et al.* 1995); $< \alpha_z >$, the mean of the distribution of local $\alpha_z \equiv \alpha(x, y)$ values (Pevtsov *et al.* 1994); α_{J_z/B_z} inferred from the slope of a least-squares linear fit to the distribution of local $J_z(x, y)$ vs. $B_z(x, y)$ values, which is closest to the definition used by Longcope and Welsch (2000) in their theoretical studies. The novel contribution of the present work is merely the demonstration that the consistency of these methods found by Leka and Skumanich applies in a statistical sense to a dataset of many active regions.

In Section 2 we find that in most (but not all) cases the main features of the SXT X-ray images in our dataset can be represented adequately using linear force-free-field extrapolations. We show that the α values from these fits to our dataset are statistically indistinguishable from those derived from photospheric vector magnetograms for the same active regions. In Section 3 we summarize our results in light of theoretical work on the continuity of currents across the photosphere and magnetic helicity conservation and reconnection in the corona.

2. X-RAY AND MAGNETIC FIELD DATA

For the purpose of this study we surveyed the full disk SXT data for active regions with relatively simple bipolar topology, in order that we might plausibly model the coronal magnetic fields with the linear force-free-field approximation. We included only regions within $\sim 45°$ of the central meridian, for which there were available both full disk coronal images from the Yohkoh SXT and full disk low resolution line of sight magnetograms from the National Solar Observatory / Kitt Peak (NSO/SP) spectromagnetograph (Jones *et al.* 1992)

that were cotemporal within ~ 1 hour. We gave priority to active regions that were observed for several days during their disk passage. The resulting data set (Table 1) includes 65 pairs of SXT images and NSO/KP magnetograms of 34 active regions observed between January 1992 and March 1994. For 24 of these 34 regions, 47 photospheric vector magnetograms obtained within a few hours of the times of the full disk data are available from the Haleakala Stokes Polarimeter (HSP, Mickey 1985). Because the HSP data were obtained primarily for those active regions that were judged at the time of observation to be likely to produce flares, the regions in the combined dataset (HSP, NSO, SXT) tend to be flare-productive. Finally, our dataset is dominated by mature active regions. The areas of 20 of the 24 regions with HSP data are either constant or decreasing at the NSO/KP times given in Table 1. Of those 4 regions that are growing in area, only two are within a few days of initial emergence: AR 7231 (~ 1 day old at 1992 October 25 14:56 UT) and AR 7150 (~ 1.5 days old at 1992 April 29 14:58 UT).

2.1. Coronal Values of α (α_c)

We co-aligned each pair of SXT images ($4.95''$ per pixel) and NSO/KP magnetograms (4-$4.5''$ per pixel), compensating for solar rotation, and the time difference. We extracted from the latter a sub-area that included all magnetic flux which the SXT images showed to be associated with that region. We did not use any NSO/KP magnetograms which showed obvious saturation effects; to the extent that there are subtle saturation effects, they will influence our results. We used the NSO/KP magnetograms to compute linear force-free fields following Gary (1989). We minimized the influence of the boundary conditions of Gary's (1989) method by extracting sufficiently large sub-areas of the magnetograms and using the SXT images to identify the full flux system of the active region.

We projected the model field lines onto the SXT image plane and visually compared them with the observed structures, adjusting the value of α by trial and error to get the best fit. The contrast of the images was enhanced to facilitate their comparison with the modeled field lines. We first plotted only field lines that originate in the areas of strong magnetic field (400–800 G). When necessary, additional field lines were selected manually in the vicinity of the coronal structures of interest. The field lines were extrapolated to a maximum height of $\approx$ 90-100 Mm. Figure 1 shows typical examples of the number and placement of field lines used to judge their match to the coronal structures. As the figure shows, the SXT images usually do not show narrow linear features that can be associated with individual loops, whatever the degree of contrast enhancement. Our approach was therefore to find the best fit to the most obvious overall structures, rather than a single linear feature. In most

cases, a single value of α_c can represent, within these uncertainties, the principal features of the active region seen in SXT images. The resulting values for each pair of SXT images and NSO/KP magnetograms are listed in the α_c column of Table 1. In some cases, different parts of the SXT image require different α_c values. Regions requiring more than one value (e.g., AR 7172 on 1992 May 23) are evident.

Figure 1 shows a region that cannot be fit with a single value of α_c. The α value that fits the upper part of the region (α_c = -1.5 $\times$ 10^{-8} m^{-1}, upper panel) is different in both amplitude and sign from the value that fits the lower part if the region (α_c = 2.1 $\times$ 10^{-8} m^{-1}, lower panel). The differences are quite evident in those field lines with footpoints in the following (negative) polarity. The value of α_c used in the upper panel results in field lines from the southern part of the negative contours that connect with weak field (below the lowest contour level) further south. The value of α_c used in the lower panel results in field lines that connect with the strong (positive) leading polarity. The shape of the southern part of the active region is not adequately fit by the alpha value and field lines shown in the upper panel.

The presence of two different values of α_c in the α_c column of Table 1 does not mean that some combination of linear force-free solutions was used to represent the magnetic field of these regions. Rather, it indicates that the overall coronal magnetic field of some active regions would be described better by a non-linear force-free model. Of course, the ability to represent images by a linear force-free model must be highly dependent on the data, as well. It would be surprising if higher-resolution coronal data did not reveal more evidence for non-linearity, given that such non-linearity is such a prominent feature of photospheric vector magnetograms.

Such visual comparison procedures are subjective, which introduces uncertainty, which we address through statistics. However, this uncertainty is of minor importance compared to the typical performance of a nominally objective procedure which imperfectly addresses all the complexities with which the judgment of an experienced data analyst can easily cope. The image attributes that are hardest for objective procedures to handle are multiple nearby structures and intensity variations within the structures themselves. Visual comparison procedures easily avoid the associated uncertainties. We have quantified the uncertainties of α_c values that arise in our procedure. First, the least difference in α that produces a visually perceptible difference in computed field lines is $\sim$ 0.3 $\times$ 10^{-9} m^{-1}. Second, some coronal features in the SXT images are rather diffuse, so all α values within a certain range produce a satisfactory fit. The uncertainty in our α_c values based on visual fitting of computed fields and the more diffuse X-ray structure is $\sim$ 1.5 $\times$ 10^{-9} m^{-1}.

For a large majority of our active regions, a linear force-free field with a single sign of

α gives a good fit to the observed coronal structures. In 53 of 65 cases (82%), a single α fit was judged to be satisfactory. In only 7 of 65 cases (11%), the X-ray structures required two different (opposite in sign) α values. As an aside, we note that only 5 out of 65 cases ($\sim$ 7%) could be fit adequately by a potential field, $\alpha_c = 0$. This is not an general result, since the regions included in our study were selected for HSP observation on the basis of their potential for flaring.

2.2. Photospheric Values of α (α_p)

We derived photospheric values of α (α_p) from the two standard types of HSP vector magnetograms, *i.e.*, half-resolution (5.6″ pixel spacing) and full-resolution (2.8″ pixel spacing). These magnetograms were derived from Stokes profiles of the spectral lines Fe I λ 6301.5 Å and λ 6302.5 Å, using nonlinear least-squares Unno-fitting (Skumanich and Lites 1987). Faraday rotation and magnetic filling factor were taken into account in the manner described by those authors. We resolved the 180° azimuthal ambiguity of the transverse field B_{trans} and computed J_z using the procedure described in the appendix of Canfield et al. (1993). Although magnetic fields in the photosphere are not force free (Metcalf *et al.* 1995), the force-free-field parameter α is a convenient measure for subsequent comparison with α_c values.

The noise level in these magnetograms is typically not more than about 100 G for transverse fields and 10 G for longitudinal ones. To take into account variations from one magnetogram to the next, the one standard deviation noise level of J_z (σ_{J_z}) was calculated for every magnetogram using a histogram of J_z values. We determined α_p using only pixels for which $B_{trans} > 300\ G$ and $J_z > \sigma_{J_z}$. The last column of Table 1 lists α_p values for all regions in our combined data set. The value of α_p for each vector magnetogram is that value of the force-free-field parameter α computed using only the pixels with vertical fields above the given thresholds that best fits the horizontal fields of the same pixels in a least squares sense. This value is called α_{best} in our original work fitting linear force-free fields to active regions magnetograms (Pevtsov *et al.* 1995) and subsequent papers. The values of α_p are within a range $\pm\ 5 \times 10^{-8}$ m^{-1}, in agreement with this earlier work, and the range has been modeled quantitatively in terms of the interaction of rising flux tubes with helical turbulent convection (Longcope *et al.* 1998).

To verify that our conclusions are insensitive to the method of calculating a single value of α for the active region as a whole, we have calculated α_{best}, $< \alpha_z >$, and α_{J_z/B_z} for each vector magnetogram. The relationships shown in Figure 2 support the conclusion of Leka & Skumanich (1999): the methods give consistent results when proper attention is paid to noise

in the data. There is somewhat less scatter in the relationship between α_{J_z/B_z} and α_{best} (lower panel) than between $<\alpha_z>$ and α_{best} (upper panel). Specifically, the Spearman correlation coefficient in the upper panel is 0.56, and the probability that there is no relationship is only 10^{-4}. In the lower panel, the correlation coefficient is even larger – 0.91 – and the probability that there is no relationship is less than 10^{-16}! This is encouraging, since α_{J_z/B_z} is used in the theoretical study of Longcope and Welsch (2000), and α_{best} is used in our past observational work. For continuity with past work, we choose to use α_{best} to measure α_p in the rest of this paper.

2.3. Photospheric and Coronal α Values Compared

Figure 3 shows the relationship between values of α determined from photospheric vector magnetograms (α_p), on the one hand, and coronal X-ray images consistent with photospheric longitudinal magnetograms (α_c), on the other. This figure shows the basic result of this paper, i.e. that α_p and α_c are equal in a statistical sense. The best linear fit (solid line) departs from the dashed line that is the locus of equality at about the 1-σ level. The best linear fit is $\alpha_c = \alpha_p(0.91 \pm 0.13) + (-0.03 \pm 0.18)$, calculated by excluding the two deviant points for which α_p is about -5.5 and 3.5 and α_c is about -1.0 and -1.5 respectively. The distribution is highly inconsistent with an uncorrelated dataset; the Spearman correlation coefficient for α_c vs. α_p is 0.71, and the probability that there is no relationship is less than 10^{-8}.

3. CONCLUSIONS

The observational results of this paper are statistically consistent with the modeling of Longcope and Welsch (2000): *the overall twist of the magnetic fields of the active regions in our dataset, which is dominated by mature active regions, is the same in the photosphere and the corona.* To reach this conclusion we have considered three different methods of calculating α_p, the overall twist of the photospheric magnetic fields of these active regions. Strengthening the earlier result of Leka and Skumanich (1999) and Leka (1999) through a database of sufficient size for significant statistics, we show that there are no important differences between these methods. In particular, α_{best}, the single value of α, based on the observed longitudinal magnetogram, that best fits the horizontal field of the corresponding vector magnetogram in a least squares sense (Pevtsov *et al.* 1995) is statistically very well related to α_{J_z/B_z}, the value of α inferred from the slope of a least-squares linear fit to the distribution of local $J_z(x,y)$ vs. $B_z(x,y)$ values, which is essentially the definition used by

Longcope and Welsch (2000) in their theoretical studies. Using α_{best}, Figure 3 shows that there is a clear correlation between α_c and α_p, and the slope of the relationship is statistically consistent with equality of these quantities in our dataset. Alternatively, one can express this result in terms of electric currents: the currents that create the steady non-potential coronal structure of these active regions pass without significant modification through the photosphere.

Our secondary conclusion is that the overall structure of the bright features in Yohkoh SXT images of the majority of the 34 active regions in our study can be represented adequately using linear force-free-field extrapolations (Section 2.1). Only 7 of our 65 cases (11%) have distinct structures in the SXT data that require more than one value of α (which turn out to be of opposite sign in most cases). We believe that the simplification of the majority of these observed structures from highly intermittent photospheric fields to a nearly linear force-free coronal field can be explained quite simply. Of course, from the r^{-3} dependence of dipolar fields one would expect that only the larger-scale components of photospheric fields will persist to large heights, and these are the fields that we tend to see in the SXT data. More significantly, however, we expect magnetic reconnection to simplify coronal structure relative to that of the underlying photosphere, in a manner analagous to Taylor relaxation in laboratory plasmas (Taylor 1974; Taylor 1986; Berger 1999). This may cause the magnetic fields of active regions to evolve toward constant α (Low 1999; Bellan 2000; Nandy *et al.* 2003) in the corona, despite the presence of large spatial variation of $\alpha(x, y)$ at their lower boundary.

We thank Dana Longcope for stimulating discussions of the analysis. NSO/Kitt Peak magnetic data used here are produced cooperatively by NSF/NOAO, NASA/GSFC and NOAA/SEL. The Yohkoh SXT instrument is a collaboration of the University of Tokyo, the National Astronomical Observatory of Japan, and the Lockheed Martin Solar and Astrophysics Laboratory. The research at MSU has been supported by NASA SR&T grant NAG5-6110.

REFERENCES

Aurass, H., Vršnak, B., Hofmann, A., and Rudžjak, V. 1999, Solar Phys. 190, 267.

Bellan, P. M. 2000, *Spheromaks: A Practical Application of Magnetohydrodynamic Dynamos and Plasma Self-Organization*, Imperial College Press, London.

Berger, M. A. 1999, Magnetic Helicity in Space Physics, in Brown, M. R., Canfield, R. C.,

and Pevtsov, A. A., editors, *Magnetic Helicity in Space and Laboratory Plasmas*, volume 111 of *Geophys. Monogr. Ser.*, pp. 1–10, Washington, D.C., AGU.

Canfield, R. C, De La Beaujardiere, J.-F., Fan, Y., Leka, K. D., McClymont, A. N., Metcalf, T. R., Mickey, D. L., Wuelser, J.-P., and Lites, B. W. 1993, ApJ 501, 853.

Gary, G. A. 1989, ApJ Supp 69, 323.

Hagyard, M. J. 1987, Solar Phys. 107, 239.

Jones, H. P., Duvall, T. L., Harvey, J. W., Mahaffey, C. T., Schwitters, J. D., and Simmons, J. E. 1992, Solar Phys. 139, 211.

Krall, K. R., Smith, J. B., Hagyard, M. J., West, E. A., and Cummings, N. P. 1982, Solar Phys. 79, 59.

Lee, J., McClymont, A. N., Mikic, Z., White, S. M., and Kundu, M. R. 1998, ApJ 501, 853.

Lee, J., White, S. M., Kundu, M. R., Mikić , Z., and McClymont, A. N. 1999, ApJ 510, 413.

Leka, K. D. 1999, Solar Phys. 188, 21.

Leka, K. D. and Skumanich, A. 1999, Solar Phys. 188, 3.

Levine, R. H. 1976, Solar Phys. 46, 159.

Longcope, D. W., Fisher, G. H., and Pevtsov, A. A. 1998, ApJ 507, 417.

Longcope, D. W. and Welsch, B. T. 2000, ApJ 545, 1089.

López Fuentes, M. C., Demoulin, P., Mandrini, C. H., and van Driel-Gesztelyi, L. 2000, ApJ 544, 540.

Low, B.-C. 1999, Magnetic Energy and Helicity in Open Systems, in Brown, M. R., Canfield, R. C., and Pevtsov, A. A., editors, *Magnetic Helicity in Space and Laboratory Plasmas*, volume 111 of *Geophys. Monogr. Ser.*, pp. 25–31, Washington, D.C., AGU.

Metcalf, T. R., Jiao, L., McClymont, A. N., Canfield, R. C., and Uitenbroek, H. 1995, ApJ 439, 474.

Mickey, D. L. 1985, Solar Phys. 97, 223.

Nandy, D., Hahn, M., Canfield, R. C., and Longcope, D. W. 2003, ApJ 597, 73.

Pevtsov, A. A., Canfield, R. C., and McClymont, A. N. 1997, ApJ 481, 973.

Pevtsov, A. A., Canfield, R. C., and Metcalf, T. R. 1994, ApJ 425, L117.

Pevtsov, A. A., Canfield, R. C., and Metcalf, T. R. 1995, ApJ 440, L109.

Pevtsov, A. A., Maleev, V. M., and Longcope, D. W. 2003, ApJ 593, 1217.

Régnier, S., Amari, T., and Kersalé, E. 2002, Astron. Astrophys. 392, 1119.

Skumanich, A. and Lites, B. W. 1987, ApJ 322, 473.

Taylor, J. B. 1974, Phys. Rev. Lett. 33(19), 1139.

Taylor, J. B. 1986, Rev. Mod. Phys. 58(3), 741.

Tsuneta, S., Acton, L., Bruner, M., Lemen, J., Brown, W., Caravalho, R., Catura, R., Freeland, S., Jurcevich, B., and Owens, J. 1991, Solar Phys. 136, 37.

Wang, T. and Abramenko, V. I. 2000, ApJ 357, 1056.

Table 1. Active Region Dataset

NOAA AR	DATE	TIME (UT) NSO/KP	SXT	HSP	α_c ($10^{-8}\mathrm{m}^{-1}$)	α_p ($10^{-8}\mathrm{m}^{-1}$)
7003	1992 Jan 09	15:34	14:36	···	-2.10	···
7008	1992 Jan 16	16:31	17:18	22:34	4.14	1.43
7008	1992 Jan 17	16:49	15:56	20:39	4.14	2.58
7008	1992 Jan 18	16:27	14:59	20:16	2.76	1.96
7029	1992 Jan 28	16:58	14:27	···	1.72	···
7029	1992 Jan 29	16:34	15:02	···	1.72	···
7029	1992 Jan 30	16:36	15:20	···	1.72	···
7033	1992 Jan 30	16:36	15:20	···	0.83	···
7033	1992 Jan 31	16:33	14:20	···	1.72	···
7056	1992 Feb 14	20:52	15:00	···	0.83	···
7070	1992 Feb 28	14:49	15:29	19:24	-0.83	-5.71
7072	1992 Feb 27	14:55	15:07	···	-0.83	···
7072	1992 Feb 28	14:47	15:29	···	-0.83	···
7072	1992 Feb 29	17:56	14:25	···	-0.83	···
7099	1992 Mar 16	16:22	16:05	23:01	1.52	0.00
7109	1992 Mar 23	14:43	15:12	17:21	-0.01	1.05
7109	1992 Mar 24	14:36	14:09	···	-0.01	···
7120	1992 Mar 30	16:21	17:45	01:52[p]	-2.62	-1.25
7123	1992 Apr 08	15:47	15:01	17:05	-2.48	0.69
7123	1992 Apr 09	15:28	13:36	00:42[f]	-2.62	-0.80
7135	1992 Apr 21	17:00	15:04	···	0.00	···
7135	1992 Apr 22	17:29	18:32	···	0.00	···
7143	1992 Apr 28	14:33	11:03	16:45	1.24	3.09
7150	1992 Apr 29	14:58	19:01	17:50	4.55	3.30
7150	1992 Apr 30	14:28	14:51	17:35	2.21	1.24
7154	1992 May 07	14:32	14:15	21:04	-2.07	-1.51
7154	1992 May 08	14:22	15:02	16:44	-2.48	-2.30
7154	1992 May 09	15:27	13:07	16:44	-2.07	-2.98
7172	1992 May 22	14:39	17:45	18:27	0.28,-0.55	0.25
7172	1992 May 23	16:02	16:58	16:31	-0.76	0.01

Table 1—Continued

NOAA AR	DATE	TIME (UT) NSO/KP	SXT	HSP	α_c (10^{-8}m^{-1})	α_p (10^{-8}m^{-1})
7172	1992 May 24	14:49	14:11	16:58	-1.03	-0.49
7216	1992 Jul 04	14:53	14:55	16:59	0.83,-0.83	-1.03
7260	1992 Aug 17	15:59	16:17	17:51	-2.48	-1.71
7260	1992 Aug 18	14:23	17:46	18:17	-1.79	-1.81
7267	1992 Aug 28	16:21	17:05	16:49	1.79	0.46
7270	1992 Sep 03	14:26	15:51	···	-0.28	···
7283	1992 Sep 23	16:00	19:54	···	-1.79	···
7293	1992 Sep 29	17:54	13:38	17:43	-1.24	3.48
7301	1992 Oct 05	15:58	16:23	17:58^{p}	0.00	1.65
7313	1992 Oct 20	18:02	18:18	···	0.00	···
7321	1992 Oct 25	14:56	16:28	00:24	1.79	0.00
7321	1992 Oct 26	16:12	16:48	17:09	1.52	2.69
7323	1992 Oct 30	17:09	14:01	22:57^{p}	0.55,0.00,-0.55	-0.06
7326	1992 Nov 01	18:59	18:02	01:28^{p}	2.48,-1.52	1.05
7326	1992 Nov 02	17:05	18:04	···	2.48,-1.52	···
7381	1992 Dec 29	16:20	16:18	19:50	0.55	0.13
7477	1993 Apr 22	13:42	14:22	17:27	1.24	0.29
7477	1993 Apr 23	14:46	16:13	17:27	0.55	0.42
7477	1993 Apr 24	14:29	14:48	18:38	0.000,1.52	0.82
7518	1993 Jun 04	13:44	14:06	18:54	-2.07	-1.25
7518	1993 Jun 05	13:59	14:27	16:43	-1.79	0..05
7518	1993 Jun 07	14:17	16:43	16:39	0.69	1.09
7588	1993 Sep 26	16:01	20:18	02:43	-0.97	-3.35
7588	1993 Sep 28	17:34	17:11	···	-1.52	···
7613	1993 Nov 02	17:16	13:01	20:47^{p}	1.24	-0.66
7613	1993 Nov 04	17:36	18:08	19:10	-1.10	0.20
7613	1993 Nov 05	16:45	18:27	17:36	-1.52	0.24
7648	1994 Jan 06	15:32	18:13	00:16	0.0	0.21
7648	1994 Jan 07	15:44	15:20	21:20	-0.55	-0.58
7648	1994 Jan 08	21:04	20:21	21:54	-0.97	-0.04

Table 1—Continued

NOAA AR	DATE	TIME (UT) NSO/KP	SXT	HSP	α_c (10^{-8}m^{-1})	α_p (10^{-8}m^{-1})
7648	1994 Jan 09	16:37	15:31	17:34	-0.28	-0.32
7648	1994 Jan 10	16:18	15:00	17:37	-0.28	-0.25
7648	1994 Jan 11	16:43	18:12	17:45	-0.55	-1.28
7685	1994 Mar 06	15:31	13:01	20:03	1.24	2.47
7685	1994 Mar 09	16:06	18:36	02:19	2.07,-1.52	0.29

[p]data for current day unavailable, value generated with data from previous day

[f]data for current day unavailable, value generated with data from following day

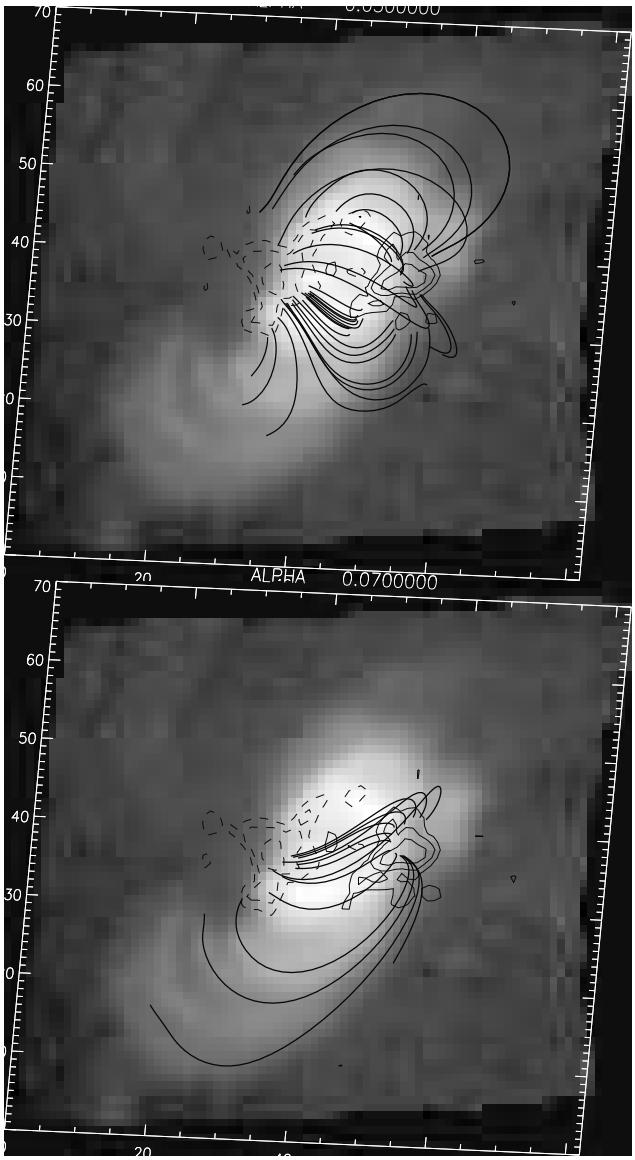

Fig. 1.— NOAA AR 7685 – a region that requires more than one α_c value. Background (greyscale) 5 x 5 $'$ image from SXT; 9 March 1994. Contours of line of sight magnetic field from NSO/KP magnetograms (dashed negative). Projected field lines from linear force-free-field extrapolation using: (upper panel) α_c = -1.5 $\times$ 10^{-8} m^{-1}. (lower panel) α_c = 2.1 $\times$ 10^{-8} m^{-1}.

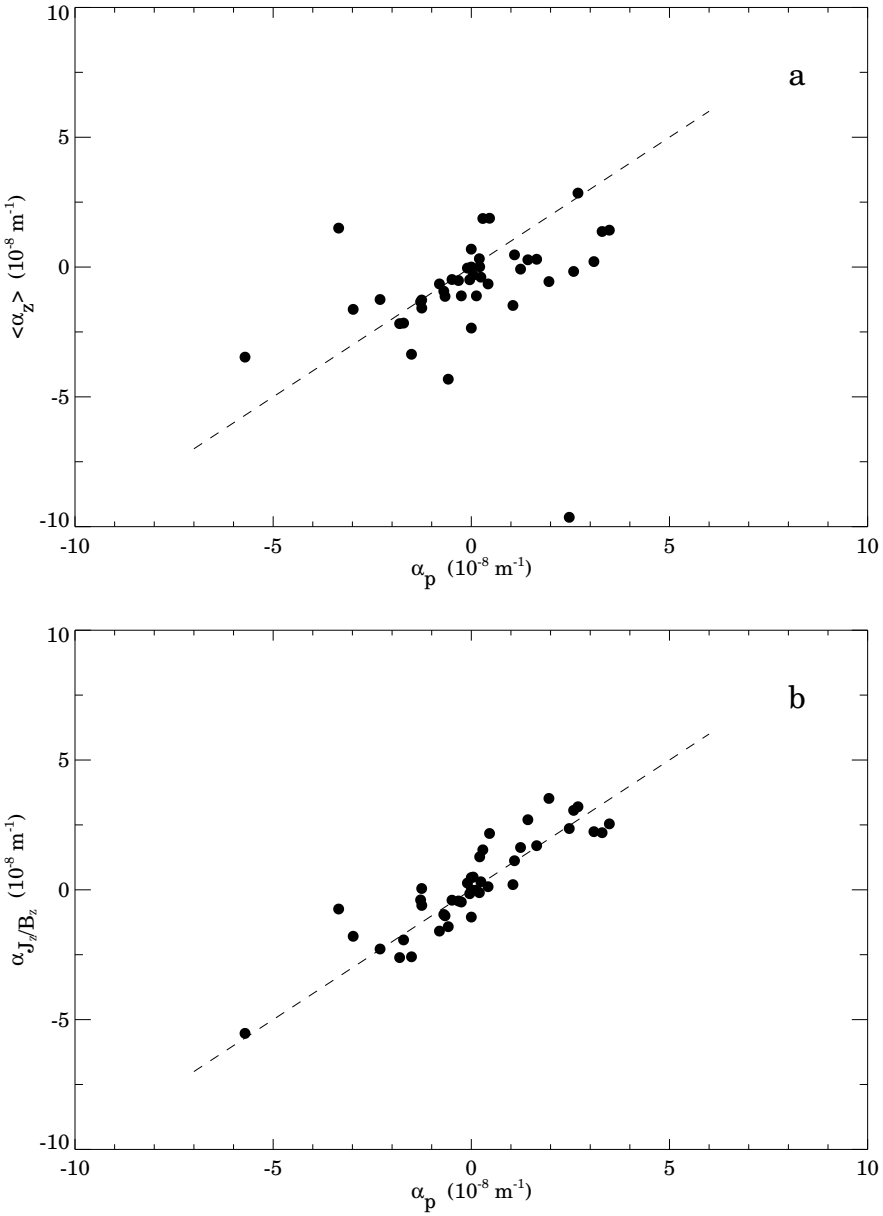

Fig. 2.— The relationship between values of the force-free-field parameter α for the regions in the combined dataset, computed by various methods. In both panels the abscissa (α_p) is α_{best} defined by Pevtsov, Canfield & Metcalf (1995). In the upper panel (a) the ordinate is $< \alpha_z >$, the mean of the distribution of local $\alpha_z \equiv \alpha(x, y)$ values (Pevtsov *et al.* 1994). In the lower panel (b) the ordinate is α inferred from the slope of a least-squares linear fit to the distribution of local $J_z(x, y)$ vs. $B_z(x, y)$ values.

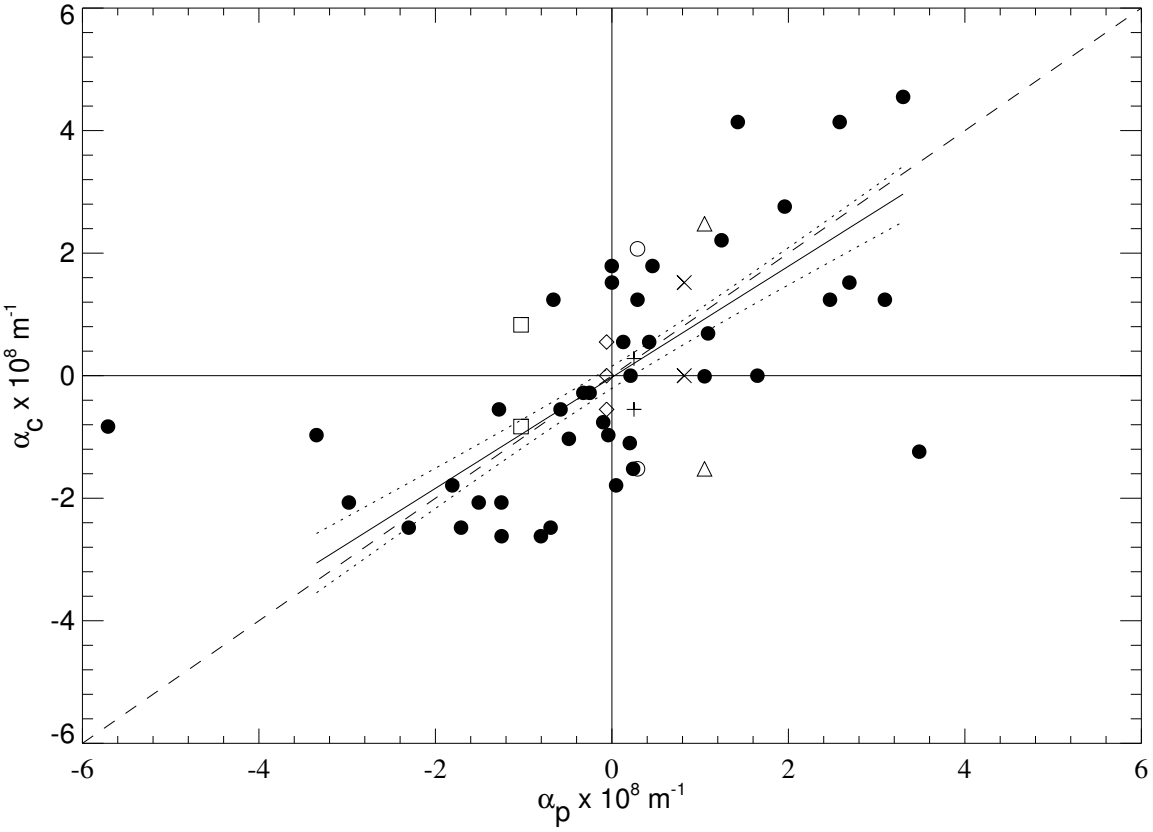

Fig. 3.— Relationship between the coronal (α_c) and photospheric (α_p) values of α for all active regions in the combined dataset. Filled circles indicate active regions adequately represented by a single α_c value. Other symbols represent the following active regions, which require more than one α_c value: + – 7172; □ – 7216; ◇ – 7323; △ – 7326; × – 7477; ○ – 7685. The solid line is a linear least squares fit to the points shown. Short-dashed lines indicate 1σ error bars. The long-dashed line is the locus of identical coronal and photospheric values.